

A universal relation for edge chipping from sharp contacts in brittle materials: A simple means of toughness evaluation

Herzl Chai^a, Brian R. Lawn^{b,*}

^a Department of Solid Mechanics, Materials and Systems, Tel Aviv University, Tel Aviv, Israel

^b Materials Science and Engineering Laboratory, National Institute of Standards and Technology, Gaithersburg, MD 20899-8500, USA

Received 28 August 2006; accepted 16 October 2006

Available online 23 February 2007

Abstract

An analysis of chipping fracture in brittle solids is presented. Cracks are introduced into the edges of selected materials, including soda-lime glass and fine-grain ceramics, using a Vickers indenter in monotonic loading. The ensuing chip morphology is examined and shown to exhibit a certain geometrical similarity, independent of material properties. A simple universal relation is derived for the critical chipping load in terms of indent location and material toughness. It is suggested that the method could be used as a simple and quick means for evaluating toughness values for glasses and fine-grain brittle materials.

© 2007 Acta Materialia Inc. Published by Elsevier Ltd. All rights reserved.

Keywords: Vickers indentation; Brittle ceramics; Edge chipping; Toughness

1. Introduction

A concentrated contact near the edge of a brittle material may lead to premature chipping. In early civilizations this fact was exploited by primitive man to fashion stone tools [1]. In the modern household, edge chipping in masonry, ceramic tiles, glass tabletops and kitchen counter-tops is a commonplace inconvenience. For this reason, edges are often rounded to avoid stress concentrations. In some cases, any such chipping that does occur may be repaired by polishing back, but this can be tedious and expensive. Edge chipping is also a central mechanism in basic material shaping, for instance glass cutting and ceramic machining [2,3]. In dentistry, chipping can cause damage to teeth and crowns, necessitating partial or full restoration. It is important to understand the basic conditions under which chipping may occur in any given brittle material.

Several attempts have been made to provide this understanding by modeling the chipping process associated with point or line loading [4–12]. Those studies cover a broad range of fracture mechanics sophistication. However, little attempt has been made to obtain specific relations for the critical chipping conditions in terms of contact location and governing material properties. From the modeling perspective, the problem is made difficult by the complex 3D nature of most chipping geometries, so that even finite element analysis is a daunting prospect except in idealized plane strain conditions. On the other hand, as we shall argue, a great deal of progress can be made by invoking the principle of geometrical similarity, enabling derivation of simple, explicit failure relations for chipping fracture.

Accordingly, in this study we conduct chipping tests on brittle materials using a Vickers indenter loaded at prescribed distances from polished orthogonal edges to deliver a monotonically increasing, normal concentrated load. The mechanics of Vickers indentation cracks in monolithic brittle materials are well documented [13,14], so it is necessary only to fold in the effects of an adjacent free surface. The

* Corresponding author.

E-mail address: brian.lawn@nist.gov (B.R. Lawn).

materials selected for testing are principally fine-grain ceramics, to avoid *R*-curve complications. Soda-lime glass is used as a model transparent material, enabling in situ viewing of the crack evolution during the entire testing, up to crack instability and beyond to ensuing spalling. We argue that the fracture pattern has a certain self-similarity, independent of indent location and material properties. This leads to the derivation of a simple, universal relation for the chipping load in terms of edge distance and material toughness. Measurements of the chipping load for all test materials, including the opaque ceramics, are subsequently made without reference to any crack measurements, and correlated in the universal relation with independently measured toughness values. It is suggested that the chipping test could be used as a simple and quick method for evaluating toughness of any given brittle material.

2. Experimental

Several brittle materials were selected for testing, in the form of rectangular plates with minimum dimensions 5 mm. Soda-lime glass was used as a model transparent solid for direct viewing of the chipping fracture process, in this case with minimum dimension 15 mm. Fine-grain polycrystalline ceramics (grain size $<5\ \mu\text{m}$) were also used: porcelain (Vita Mark II, Vita Zahnfabrik, Bad Sackingen, Germany); a dry-pressed glass-infiltrated alumina (InCeram, Vita Zahnfabrik, Bad Sackingen, Germany); Y-TZP zirconia (Lava Frame, 3M ESPE, Morrow, GA). Top and front surfaces were diamond-polished to $1\ \mu\text{m}$ finish, leaving sharp edges for indentation testing. Toughness values of these materials were independently measured from the size of radial cracks around Vickers indentations on specimen top surfaces well away from the edges [14], and are shown in Table 1.

The test configuration used to cause chipping is shown schematically in Fig. 1. A heavy duty Vickers diamond indenter was used in the crosshead of an Instron testing machine (Instron 4501, Instron Corp., Canton, MA) to apply monotonically increasing normal loads P up to 600 N at prescribed distances h up to 2.5 mm from the front face, with pyramidal diagonals parallel and perpendicular to the specimen edges. Load was applied monotonically at a rate $\approx 1\ \text{N s}^{-1}$, so that chipping occurred typically within 1–2 min. In the glass specimens, a video camera was used to follow the crack depth as a function of load, from both the side and front as well as from below. In all materials, dimensions C (depth) and D (width) of the ultimate chips on the front walls, and the critical failure loads P_F to spall these chips, were recorded.

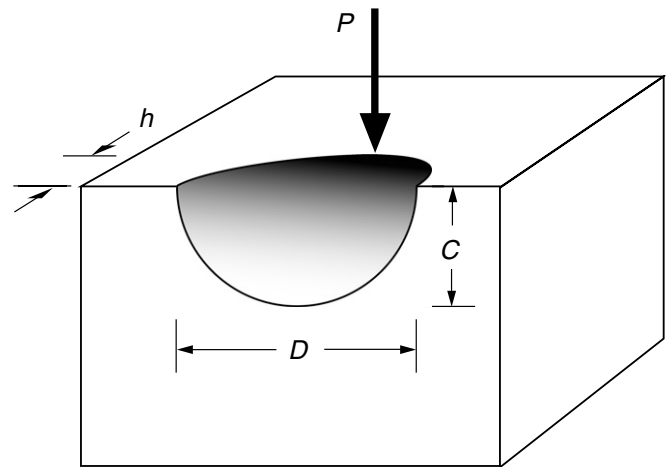


Fig. 1. Schematic of scallop-shaped chip formation in brittle material. P is load on Vickers indenter, h is distance of indentation center from the front face, c is crack depth below top surface (not shown), and C and D are spall dimensions. Cracks are viewed from below the contact and from the front and side faces.

3. Results and analysis

3.1. Chipping morphology

A video sequence from a subsurface-view camera of a glass specimen during Vickers indentation at a distance $h = 1.05\ \text{mm}$ from the front face is shown in Fig. 2a–d. The Vickers indentation initially formed two mutually orthogonal sets of radial–median crack arms [15], one parallel and one perpendicular to the front surface. At relatively low load $P = 62\ \text{N}$, Fig. 2a, the cracks have just begun to extend. On increasing the load to $P = 120\ \text{N}$, Fig. 2b, the parallel crack has extended laterally and slightly toward the specimen edge. At higher load $P = 176\ \text{N}$, Fig. 2c, the lateral extension and curvature are more developed. At $P = 190\ \text{N}$, Fig. 2d, the crack is on the verge of failure. Finally, at $P = 191\ \text{N}$, Fig. 2e, the crack (here viewed postmortem from the top surface) has intersected the front free surface to form a chip of width $D \approx 7.6\ \text{mm}$. This surface chip geometry has been well described in an earlier study by Lardner et al. [7]. The “attractive” influence of the free surface on the crack trajectory is manifest. Note that the perpendicular crack arm extending away from the front face (upward in Fig. 2) has barely grown, indicating comparatively little interaction with the free surface.

Fig. 3 contains video clips from a side-view camera for another crack also distant $h = 1.05\ \text{mm}$, showing the downward evolution of the median crack system. The parallel median crack is seen as the dark shadow, the smaller perpendicular crack as the very faint circular fringe pattern. At $P = 104\ \text{N}$, Fig. 3a, the crack has undergone small downward extension. On increasing the load to $P = 160\ \text{N}$, Fig. 3b, the parallel crack begins to outpace its perpendicular counterpart. At $P = 200\ \text{N}$, Fig. 3c, the initially parallel crack begins to curve around, predominantly near the

Table 1
Toughness K_{IC} ($\text{MPa m}^{1/2}$) of materials used in this study

Glass	Porcelain	Alumina	Y-TZP
0.6	0.9	2.5	3.7

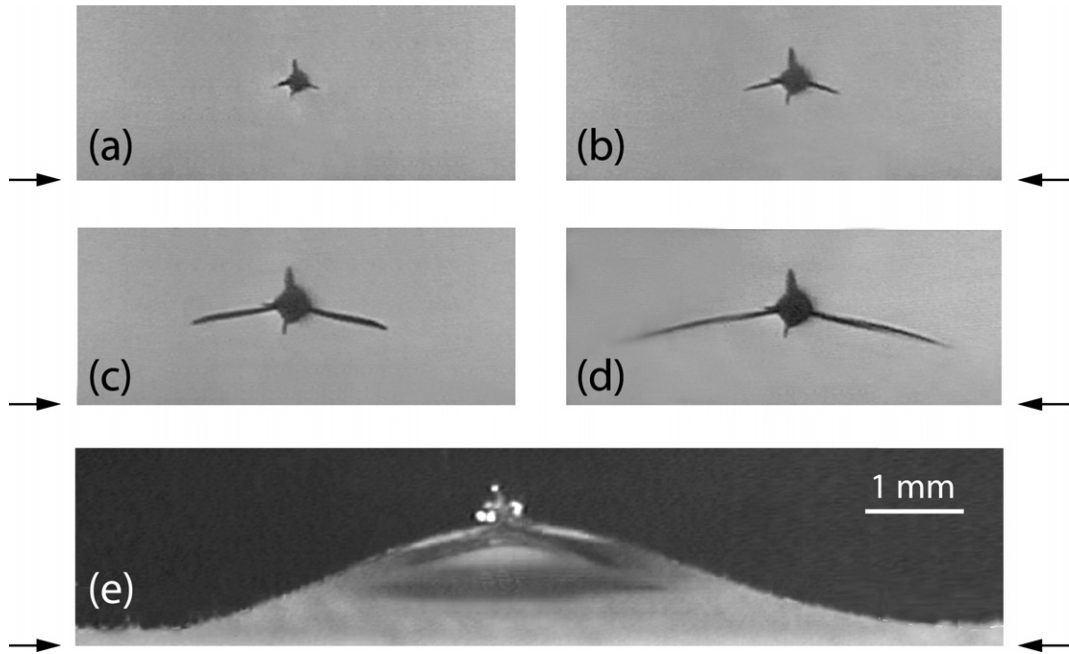


Fig. 2. Chip on top surface of soda-lime glass formed by Vickers indenter at distance $h = 1.05$ mm from front surface (indicated by arrows), subsurface views, at loads: (a) $P = 62$ N, (b) $P = 120$ N, (c) $P = 176$ N, (d) $P = 190$ N, (e) $P = 191$ N (postmortem view). Chip forms from crack arms initially parallel to front surface. Crack arms perpendicular to front surface are relatively unaffected.

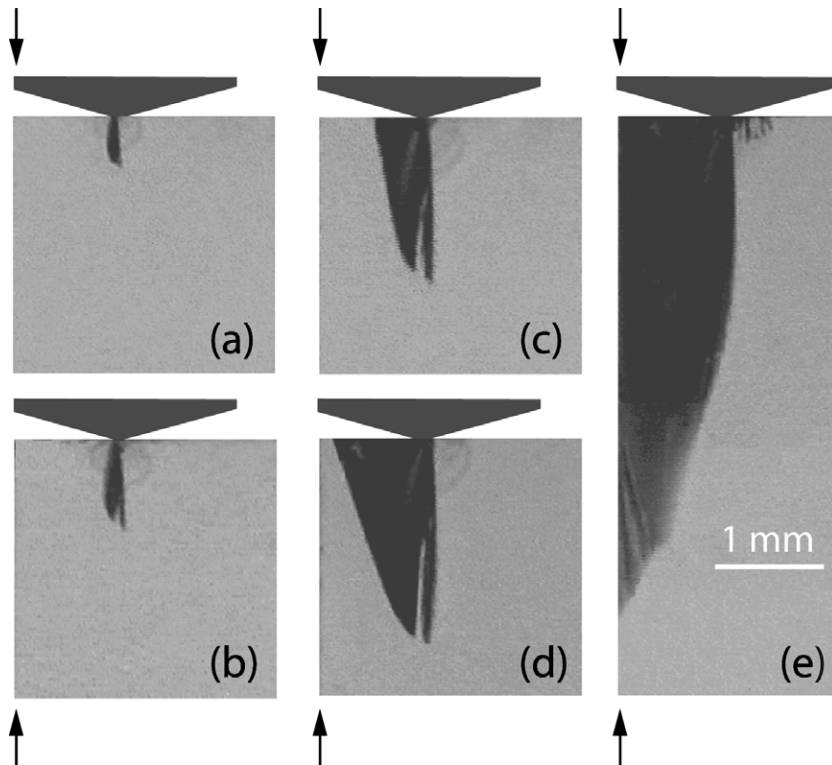


Fig. 3. Video sequence showing evolution of Vickers crack at distance $h = 1.05$ mm from front surface (indicated by arrows), side-on views, at loads: (a) $P = 100$ N, (b) $P = 160$ N, (c) $P = 200$ N, (d) $P = 204$ N, (e) $P = 205$ N. Primary median crack seen as dark shadow, smaller secondary (orthogonal) median crack as faint fringe pattern.

top surface (cf. Fig. 2), accounting for a broadening of the dark shadow. A further slight increase in load to $P = 204$ N, Fig. 3d, rapidly accentuates this deepening

and broadening. At this point the crack has reached a critical depth $c_F = 1.8$ mm, i.e. is on the verge of instability. Finally, with an infinitesimal increment in load to

$P = P_F = 205$ N, Fig. 3e, the crack has become unstable and accelerated into a familiar conchoidal spall of depth $C = 4.2$ mm.

Fig. 4 is an analogous sequence, from a front-view camera for another test in glass, at $h = 0.63$ mm. This time the parallel crack is visible as the faint fringe pattern, the perpendicular crack as the much smaller dark line. The parallel crack begins in its classical median configuration at $P = 65$ N, Fig. 4a, with downward and lateral expansion at $P = 77$ N, Fig. 4b. With further slight increase in load to $P = 78$ N, Fig. 4c, the crack expands rapidly, and is on the verge of instability at depth $c_F = 1.3$ mm. Spallation on the front face occurs in the next crack increment at $P = P_F = 79$ N, Fig. 4d, to spall depth $C = 3.0$ mm and width $D = 5.6$ mm.

The kind of fracture evolution described in Figs. 2–4 cannot be followed in the opaque ceramics. However, it is straightforward to determine the final chip morphology from the spall dimensions on the front face. Plots of C versus h and D versus h are shown in Fig. 5a and b. Note that the data can be represented by linear fits, independent of material. This implies a certain geometrical similarity in the chipping process. Regression of the data in Fig. 5 yields $C/h = 5.1$ and $D/h = 8.0$.

3.2. Fracture mechanics

Consider a sharp-indenter median crack of depth c located distance h from the front face, Fig. 1. For $c \ll h$, the specimen may be approximated by a semi-infinite solid, where the stress-intensity factor K has the well-documented form [13,16,17]

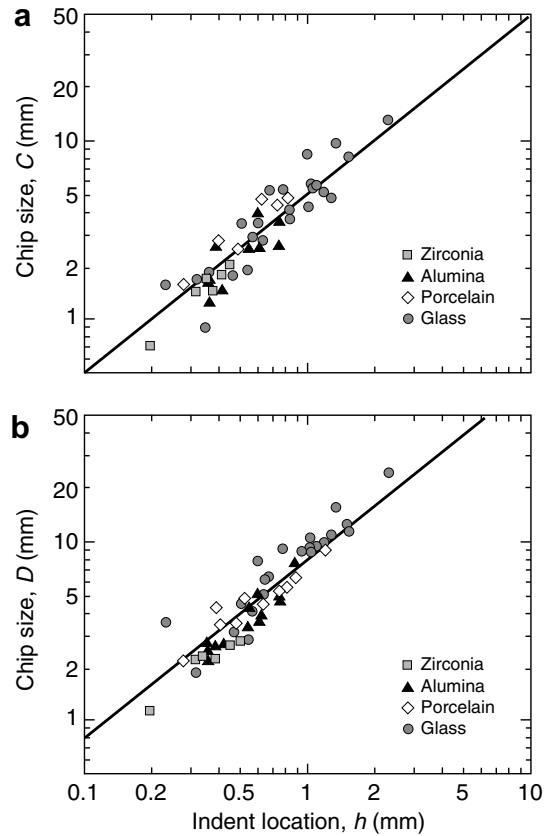


Fig. 5. Plot of: (a) depth C and (b) width D of median crack as function of indenter location h relative to specimen edge. Data for selected glass and ceramics overlap, indicating geometrical similarity. Solid lines are linear fits $C/h = 5.1$ and $D/h = 8.0$.

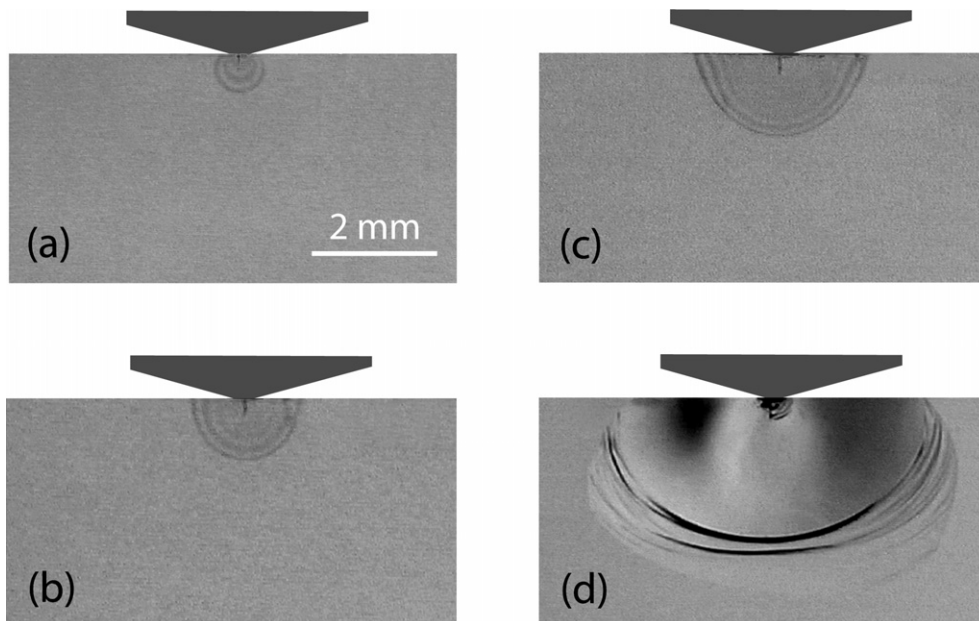


Fig. 4. Video sequence showing evolution of Vickers crack at distance $h = 0.63$ mm from front surface, front-on views, at loads: (a) $P = 65$ N, (b) $P = 77$ N, (c) $P = 78$ N, (d) $P = 79$ N. Primary median crack seen as faint fringe pattern, smaller secondary (orthogonal) median crack as dark shadow.

$$K = \chi_e P / c^{3/2} = K_c \quad (1)$$

at equilibrium, where K_c is the toughness and χ_e is an indentation coefficient relating to the elastic component of the indentation field [17]. It is assumed that K_c is single-valued and crack-size independent, which is valid for fine-grain materials without R -curve behavior [18]. It is also assumed that the indenter does not unload prior to chipping, in which case a residual inelastic component in the indentation stress field may be neglected [17]. As crack-size increases, the influence of the front free surface will begin to be felt. We may accommodate this influence by normalizing crack size c relative to indent location h and transforming Eq. (1) to obtain

$$P/h^{3/2} = (K_c/\chi_e)(c/h)^{3/2}f(c/h) \quad (2)$$

where $f(c/h)$ is a dimensionless function, with $f(c/h) = 1$ in the limit $c/h = 0$. Noting the geometrical similarity implied in Fig. 5, we may expect $f(c/h)$ to be material-independent.

For glass, where the crack can be followed throughout its evolution, the $P(c)$ dependence can be explored in detail. Accordingly, Fig. 6 plots $P/h^{3/2}$ as a function of c/h for glass. Each data symbol represents a different crack, for h values ranging between 0.2 mm and 2 mm. The solid curve is an empirical fit through the data. The inclined dashed line is the asymptotic limiting case $f(c/h) = 1$ in Eq. (2). Above $c/h \approx 0.5$ the data begin to deviate away from this line, bending over and passing through a maximum $P_F/h^{3/2} \approx 5.8 \text{ MPa m}^{1/2}$ at $c_F/h \approx 2.0$. Beyond this point the crack becomes unstable, corresponding to chipping failure. The critical load condition for failure in Eq. (2) then takes the general form

$$P_F/h^{3/2} = \beta K_c \quad (3)$$

where $\beta = (1/\chi_e)(c_F/h)^{3/2}f(c_F/h) = \text{constant}$, independent of material.

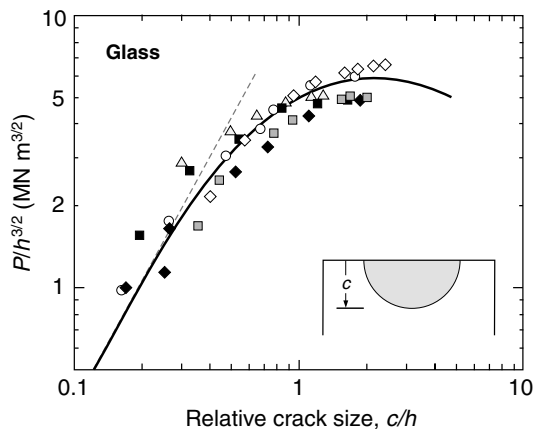


Fig. 6. Plot of $P/h^{3/2}$ as a function of c/h for soda-lime glass, describing median crack evolution to chipping failure. Each data symbol represents a different crack, for h in the range 0.2–2 mm. Solid curve is an empirical fit through the data. Inclined dashed line is the asymptotic limiting case $f(c/h) = 1$ in Eq. (2). Note maximum in curve, defining critical fracture condition.

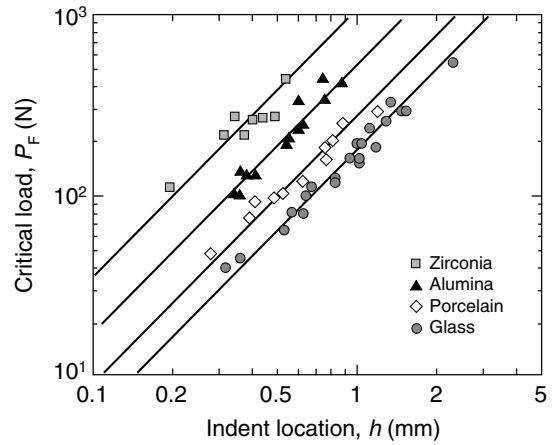


Fig. 7. Plot of chipping load P_F versus indentation distance h for selected glass and ceramic materials. Solid lines represent best fits of Eq. (2).

Whereas in the case of opaque ceramics it is difficult to obtain $P(c)$ data, measurement of P_F is straightforward. A plot of P_F versus h for each test material is given in Fig. 7. Regression fits of Eq. (3) to each data set, with force-fit slopes 1.5 (logarithmic coordinates), are then made to determine values of βK_c . Soda-lime glass is the best-characterized of our test materials, so let us take it as our reference baseline. Reproducible crack velocity $v(K)$ curves have been well documented for this material by Wiederhorn for tests in moist atmospheres [19,20], so we can specify an independent, accurate value of effective K_c from a knowledge of the crack growth rate. From observations such as those in Figs. 2–4, in conjunction with the known load rate $\approx 1 \text{ N s}^{-1}$, we estimate a crack velocity of $\approx 0.1 \text{ mm s}^{-1}$ near the instability point, corresponding to an effective toughness $K_c = 0.6 \pm 0.1 \text{ MPa m}^{1/2}$ for soda-lime glass from Wiederhorn’s $v(K)$ curves. The regression fit to the glass data yields $\beta K_c = 5.6 \pm 0.8 \text{ MPa m}^{1/2}$ (mean and standard deviation), corresponding to a value $\beta = 9.3 \pm 1.3$. With this calibration, K_c values can now be

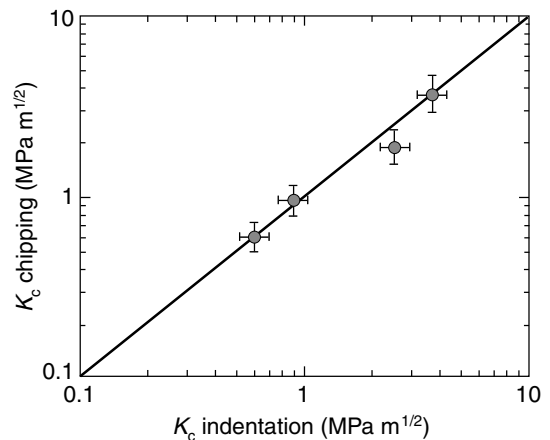


Fig. 8. Plot of toughness K_c for selected glass and ceramic materials, showing values estimated from Eq. (3) versus values determined from conventional Vickers indentation measurements.

determined from the regression fits for the other materials. These values are plotted in Fig. 8 as a function of indentation toughness determined from independent, conventional Vickers indentation tests. Notwithstanding the scatter in data, the fit in this plot confirms a direct correlation between critical chipping conditions and toughness for the materials tested here.

4. Discussion

We have investigated edge chip formation in brittle solids using a sharp indenter located at prescribed distances h from the edges of homogeneous glasses and ceramics, i.e. materials characterized by a single-valued toughness K_c . In our tests we have used a Vickers indenter, but a Knoop indenter would work equally well. The indentation creates orthogonal radial–median cracks along the indentation diagonals, in our case oriented parallel and perpendicular to the edges. The crack parallel to the edge dominates, propagating downward and toward the front surface and resulting in a chipping scallop at a critical load P_F . The chip morphology exhibits a certain geometrical similarity, independent of material, with characteristic depth and width dimensions on the front face $C \approx 5h$ and $D \approx 8h$ (Fig. 1). This corresponds to a chip volume $V \approx \pi CDh/6 \approx 21h^3$, demonstrating that a contact close to a sharp edge can remove a large quantity of material.

The power of the geometrical similarity argument is that it enables specification of the universal critical load relation in Eq. (3) in the simplest way, essentially based on dimensional analysis. This approach circumvents the need for a detailed fracture mechanics derivation of the function $P(c)$. Such a detailed derivation is impractical, even by finite element analysis, because of the 3D complexity of the problem. The simplifying feature in the present approach is the scaling of the critical depth c_F for chipping with the contact location h , independent of material, leading to the $P_F \propto h^{3/2}$ dependence evident in Fig. 7.

A feature of the analysis is the interrelation between critical load P_F and toughness K_c in Eq. (3). This provides a simple means of estimating K_c directly from chipping loads, to within an accuracy of about 25%. Part of the uncertainty arises from variation in experimental repeatability, part from scatter in the independent measurements of K_c [14]. As indicated, it is easy to measure critical loads P_F in opaque ceramics. One only needs specimens with polished edges and minimum dimensions larger than about twice the chip size (typically 5 mm) and access to a heavy duty Vickers indenter. It is unnecessary to measure any crack size c ; the only dimension needing measurement is indent location h . In this sense, the chipping test is easier even than the conventional Vickers indentation fracture test in which K_c is measured from radial crack dimensions [14]. Interestingly, the maximum in Fig. 6 is reminiscent of two-step indentation–strength tests where indentations are placed into flexure specimens and the

strength is subsequently measured [21]. It is as if the free surface in the chipping test, by removing constraining bulk material, were imposing a “fictitious” tensile stress on the crack.

Finally, as with all tests, the chipping test described here is not without its limitations: (i) We have indicated that crack growth in brittle ceramics is subject to rate effects, especially in moist environments, according to some velocity relation. Such effects are well known in indentation tests, where radial cracks can grow steadily at (or even after) loading [22]. Rate effects been observed too in the current chipping tests in glass; median cracks continue to grow toward instability after the load has been halted. In Fig. 6, this is equivalent to crack growth along a horizontal line at constant P toward the instability branch of the $P(c)$ function. Ignoring such rate effects will lead to underestimates of the true equilibrium value of K_c . (ii) The fine-grain ceramics selected for study here have a single-valued toughness, i.e. no significant R -curve [18,23]. In large-grain ceramics with heterogeneous microstructures, R -curve behavior will become evident. The measured K_c will then be that corresponding to the crack length at failure. In such materials crack growth becomes somewhat more stable because the effective toughness increases with extension, and the bridged paths will become less smooth as the crack front undergoes enhanced deflection [18], i.e. crumbling rather than chipping. (iii) We have considered only monotonic loading, as befits most chipping events. This avoids any complications associated with unloading and repeated reloading, which can further accelerate cracks owing to the action of residual stresses around hardness impressions [17] and fatigue effects [24]. (iv) It is implicit in Eqs. (1)–(3) that two conditions be met: first, that median cracks initiate at a low load; and second, that they extend well beyond the immediate plastic contact zone. In most brittle materials, the initiation threshold occurs at much lower loads than the critical values P_F measured here [25]. To guarantee the second condition, it is necessary only to ensure that h (here ≈ 1 mm) is larger than the indentation size ($\approx 100 \mu\text{m}$). In this limit, the critical conditions will be insensitive to contact type, e.g. Vickers or Knoop. (v) We have considered only normal loading. The imposition of a tangential component in the loading will influence the crack trajectory and hence critical chipping load in Eq. (3).

Acknowledgements

This work was supported by a grant from the US National Institute of Dental and Craniofacial Research (PO1 DE10976).

Certain equipment, instruments or materials are identified in this paper in order to adequately specify the experimental details. Such identification does not imply recommendation by the National Institute of Standards and Technology, nor does it imply the materials are necessarily the best available for the purpose.

References

- [1] Cotterell B, Kaminga J, Dickson FP. *Int J Fracture* 1985;29:205.
- [2] Jahanmir S. *Mach Sci Technol* 2004;2:137.
- [3] Scieszka SF. *Tribol Int* 2005;38:834.
- [4] McCormick NJ. *Metal Mater* 1982;8:154.
- [5] Almond EA, McCormick NJ. *Nature* 1986;321:53.
- [6] Thouless MD, Evans AG, Ashby MF, Hutchinson JW. *Acta Metall* 1987;35:1333.
- [7] Lardner TJ, Ritter JE, Shiao ML, Lin MR. *Int J Fracture* 1990;44:133.
- [8] Chui WC, Thouless MD, Endres WJ. *Int J Fracture* 1998;90:287.
- [9] Quinn JB, Su L, Flanders L, Lloyd IK. *Mach Sci Technol* 2000;4:291.
- [10] Morrell R, Gant AJ. *Int J Refract Metal Hard Mater* 2001;19:293.
- [11] Morrell R. *Key Eng Mater* 2005;290:14.
- [12] Gogotsi G. *Inorg Mater* 2006;42:567.
- [13] Marshall DB, Lawn BR. *J Mater Sci* 1979;14:2001.
- [14] Anstis GR, Chantikul P, Marshall DB, Lawn BR. *J Am Ceram Soc* 1981;64:533.
- [15] Lawn BR, Swain MV. *J Mater Sci* 1975;10:113.
- [16] Lawn BR, Fuller ER. *J Mater Sci* 1975;10:2016.
- [17] Lawn BR, Evans AG, Marshall DB. *J Am Ceram Soc* 1980;63:574.
- [18] Swanson PL, Fairbanks CJ, Lawn BR, Mai Y-W, Hockey BJ. *J Am Ceram Soc* 1987;70:279.
- [19] Wiederhorn SM, Bolz LH. *J Am Ceram Soc* 1970;53:543.
- [20] Wiederhorn SM. In: Bradt RC, Lange FF, Hasselman DPH, editors. *Fracture mechanics of ceramics*. New York: Plenum; 1974. p. 613.
- [21] Chantikul P, Anstis GR, Lawn BR, Marshall DB. *J Am Ceram Soc* 1981;64:539.
- [22] Jakus K, Ritter JE, Choi SR, Lardner T, Lawn BR. *J Non-Cryst Solid* 1988;102:82.
- [23] Swanson PL. In: Varner J, Frechette VD, editors. *Fractography of glasses and ceramics*. Columbus, OH: American Ceramic Society; 1988. p. 135.
- [24] Guiberteau F, Pature NP, Cai H, Lawn BR. *Philos Mag A* 1993;68:1003.
- [25] Lawn BR, Marshall DB. *J Am Ceram Soc* 1979;62:347.